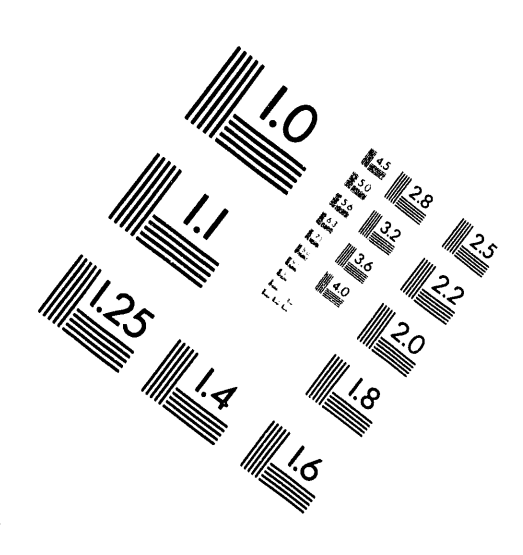
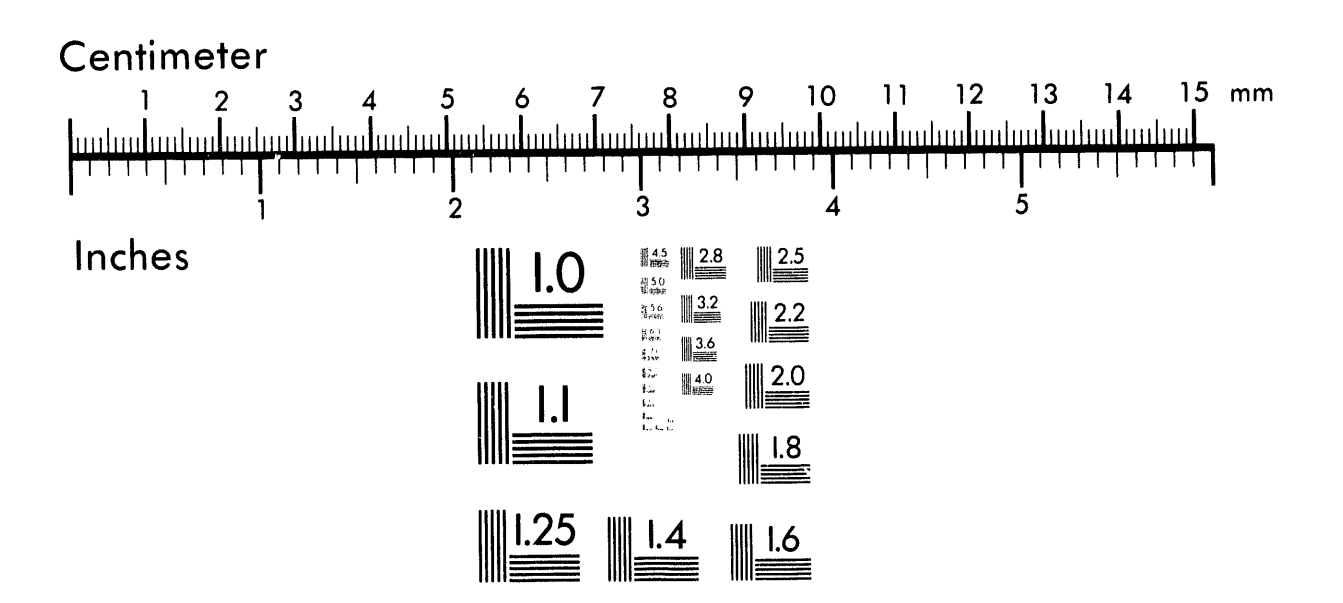


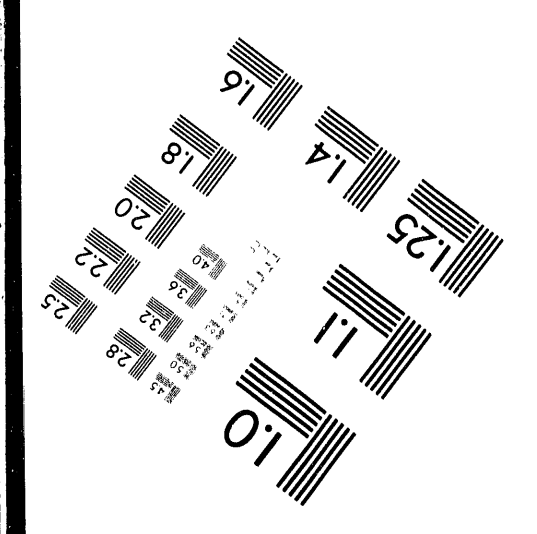


### **Association for Information and Image Management**

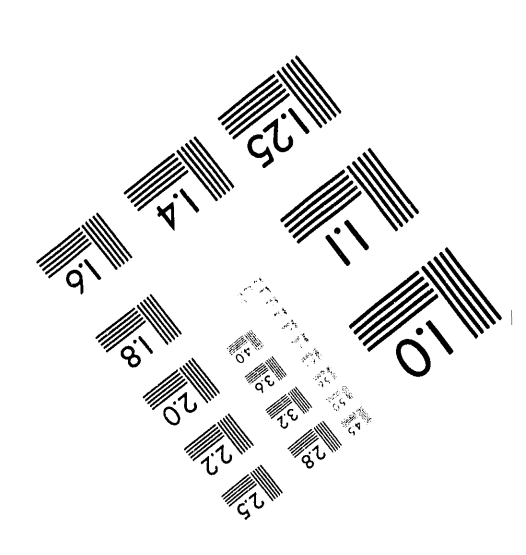
1100 Wayne Avenue, Suite 1100 Silver Spring, Maryland 20910 301/587-8202



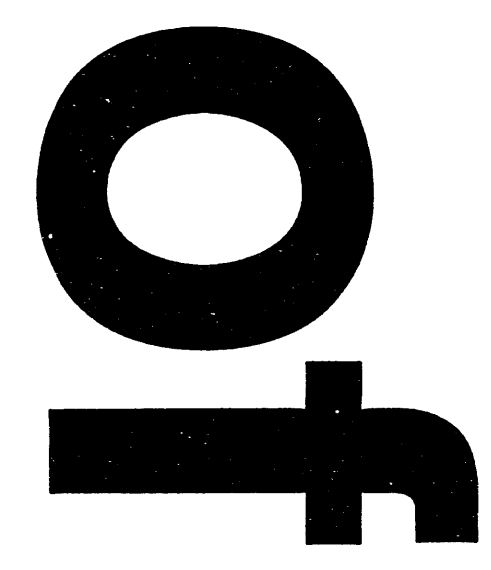




MANUFACTURED TO AIIM STANDARDS
BY APPLIED IMAGE, INC.







# N-9510135--4

PNL-SA-22546

# **DISCLAIMER**

This report was prepared as an account of work sponsored by an agency of the United States Government. Neither the United States Government nor any agency thereof, nor any of their employees, makes any warranty, express or implied, or assumes any legal liability or responsibility for the accuracy, completeness, or usefulness of any information, apparatus, product, or process disclosed, or represents that its use would not infringe privately owned rights. Reference herein to any specific commercial product, process, or service by trade name, trademark, manufacturer, or otherwise does not necessarily constitute or imply its endorsement, recommendation, or favoring by the United States Government or any agency thereof. The views and opinions of authors expressed herein do not necessarily state or reflect those of the United States Government or any agency thereof.

October 1993

REPRESENTING THE INFLUENCE OF SUBGRID TOPOGRAPHY ON HYDROLOGY

Richland, October 0 and the Symposium on Environment 19-21, 1993 Heal th

under U.S. Department of Energy or Contract DE-AC06-76RLO 1830

Pacific Northwest Laboratory Richland, Washington 99352

0 1993

### Representing the Influence of Subgrid Topography on Hydrology

L. Ruby Leung and Steven J. Ghan

Pacific Northwest Laboratory, Richland, WA 99352

Tel: (509)-376-0594 Fax: (509)-376-5217

KEY WORDS: Regional climate model, aggregation method, topography, cloud, precipitation, snow cover

### **ABSTRACT**

Estimates of the impact of global climate change on land surface hydrology require climate information on scales far smaller than those explicitly resolved by global climate models of today and the foreseeable future. To bridge the gap between what is required and what is resolved, we propose a subgrid-scale parameterization of the influence of topography on clouds, precipitation, and land surface hydrology. The parameterization represents subgrid variations in surface elevation in terms of discrete elevation classes. Separate cloud and surface processes are calculated for each elevation class. The simulated surface temperature, precipitation, snowpack, and soil moisture for each elevation class can then be distributed according to the spatial distribution of surface elevation within each grid cell. The scheme is being applied to the Pacific Northwest Laboratory's climate version of the Penn State/NCAR Mesoscale Model. Validation is being addressed by driving the model with observed lateral boundary conditions for the Pacific Northwest and comparing with surface observations. Preliminary results from the simulation will be presented.

### 1. INTRODUCTION

Human activities rely critically on the distribution of surface moisture and precipitation. These, together with water vapor and cloud in the atmosphere and snow cover on the ground surface, constitute the hydrological cycle that interacts intimately with the atmosphere-ocean system. An understanding of the impacts of global climate change on human society cannot neglect these complicated interactions. Yet it is this component that, at present, represents the most uncertainty in the modeling of the global environment.

The modeling of climate has evolved from simple 1- or 2-dimensional models that capture the energy balance of the climate system to complicated 3-dimensional models that couple the atmosphere and ocean with rather detailed physical parameterizations. However, because of the diversity of spatial and temporal scales involved in hydrological processes of the atmosphere and the land surface, global climate models (horizontal resolution of a few hundred kilometers) are far from being able to model these processes at scales useful for impact assessment (less than ten kilometers).

One example is the modeling of precipitation. Evaluation of a number of General Circulation Models (GCM) performed by the Intergovernmental Panel on Climate Change (IPCC, 1991) indicated that there is an error between 20-50% in the model simulated seasonal precipitation when compared with observations averaged over regions of roughly 15° by 15°. Furthermore, sensitivity studies using a number of GCMs in a doubled  $CO_2$  concentration experiment reveal that, on regional scales, the differences in the projected changes in seasonal precipitation are of the same order of magnitude as the change themselves (Grotch and MacCracken, 1991).

Undoubtedly, such disparity between model results and observations are due to both an insufficient understanding or representation of the physical processes and a lack of horizontal resolution to resolve either the atmospheric dynamics or the characteristics of the lower boundary such as land surface and topography. In an effort to test the advantage of using higher horizontal resolution in climate models, Giorgi et al. (1989,

1993) developed a regional climate model and used it to simulate climatology over the western U.S. With more detailed parameterizations of cloud and much higher horizontal resolution (60 km) compared with GCMs, their studies indeed show improvements in skill for simulating seasonal precipitation on the regional scale (several hundred kilometers). However, differences between the simulated and observed precipitation remain significant when comparisons were made on scales less than 100 km (Giorgi et al., 1992). This suggests that two areas of research are still needed to bring the model simulation of the hydrological cycle to closer agreement with observations on spatial scales useful for climate change studies. First, improvements in physical parameterizations of the processes in the atmosphere that govern the hydrological cycle are needed. Second, parameterizations that account for the subgrid variations due to unresolved dynamics and lower boundary are essential even in regional climate models. This paper represents an early effort targeting at the latter: to develop a parameterization of subgrid orographic precipitation for climate models.

Topography is a prominent feature in the western U.S. An accurate simulation of precipitation in this area cannot be achieved without considering the effects of topography on precipitation. This is particularly true for explaining the spatial distribution of precipitation along coastal mountain ranges (e.g. Smith, 1987; Sumner, 1988). During winter time, precipitation is often generated as a result of the lifting of the moisture-rich air by the elevated surface below. Condensation and subsequent evolution of clouds are controlled by more detailed air circulations and cloud microphysical processes. Past studies indicated an enhancement between 50-80% in precipitation by hills up to a few hundred meters high (Browning 1980; Storebo, 1975, Hobbs et al., 1973). For mountains above 1-2 km, the enhancement can be more than 200% (Barros and Lettenmaier, 1993). The accumulation of snow on mountain peaks affects water resources over large geographical areas covered by the river drainage system. The capability of climate models to capture these climatological features are essential to an integrated modeling of the changing environment.

Barros and Lettenmaier (1993) reviewed and summarized a list of mechanisms that are identified from numerous previous studies (e.g., Hobbs et al., 1973; Fraser et al., 1973;

Choularton and Perry, 1986) to be important to the generation of orographic precipitation. Among those are the general dynamics of air flow over mountain barriers and cloud microphysical processes such as the seeder-feeder mechanisms (Bergeron, 1960; Browning et al., 1975). The former has more prevailing influence on long term precipitation distributions. We have developed our parameterization scheme based on a simple air-flow model and a detailed mixed-phase cloud microphysics model to represent the above two components. To seek a balance between detailed physical representations and computational efficiency for climate applications, we have adopted an aggregation approach that represents the variations of surface elevation with a limited number of surface elevation classes. The model formulation will be described in Section 2 that follows. The parameterization has been implemented into a regional climate model. Precipitation is simulated for all surface elevation classes within the grid cells of the model and distributed back to its geographical locations. Other aspects of the hydrological cycle, namely soil moisture, snow accumulation, and surface evapotranspiration, are also accounted for in the subgrid scale in this framework. Model results and sensitivity tests will be discussed in Section 3.

### 2. MODEL DESCRIPTION

Following the approach pioneered by Dickinson et al., (1989) and Giorgi et al., (1989), a regional climate model has been developed at the Pacific Northwest Laboratory (PNL) based on the Penn State/NCAR Mesoscale Model (MM4) (Anthes et al., 1987). Several physical parameterizations important on climatic time scales have been implemented into the model. They are equivalent to those used in the PNL version of the NCAR Community Climate Model (CCM1) (Williamson et al., 1987). The use of the same physical parameterizations in both regional and global models also facilitates their future coupling for climate change studies. These parameterizations include a two-stream delta-Eddington treatment for shortwave radiation (Taylor and Ghan, 1992) and an emissivity approach for longwave radiation (Kiehl et al., 1987); a bulk cloud microphysics scheme that distinguishes liquid and ice phase (Cotton et al., 1986; Ghan and Easter, 1992); and a surface physics scheme (BATS1E) (Dickinson et al., 1993). A split-explicit time integration scheme with efficient treatment of gravity waves (Madala, 1987) has been introduced in this version of MM4. It permits the use of a 6-minutes time-step for simulations with a

horizontal resolution of 90 km. Grell's parameterization scheme (Grell, 1993) is used for treatment of cumulus convection. For the planetary boundary layer, the high-resolution model of Zhang and Anthes (1982) is used.

In mesoscale models, high horizontal resolutions are generally achieved through the use of nesting. As the horizontal resolution increases, shorter time steps and more spatial points in the simulation place a significant burden on computational requirements. Therefore, most models of orographic precipitation in the past are developed for the purpose of gaining understanding of the physical processes rather than for climate applications. Most of them have detailed air circulation as well as cloud microphysics schemes and require time steps of a few seconds (e.g. Fraser et al., 1973; Tripoli and Cotton 1986). To explicitly resolve the often highly varying surface elevations in the continents would therefore not be very feasible, particularly on climate time scales. We have adopted an alternative method based on aggregation of surface elevation. Subgrid variations in surface topography are represented by a limited number of surface elevation classes. The 12 categories used to define the surface elevation classes are shown in Table 1. From a surface topography dataset of 1.5 km resolution, information relating to the aggregation scheme is derived. This include, for each grid cell of a model domain, the grid-cell mean surface elevation, the number of elevation classes it contains, the mean elevation of those areas belonging to the same elevation class, and the fraction of area covered by each elevation class. On average, 4.5 classes are carried by each 90-km grid cell over the continental U.S.

There are two main components in the subgrid parameterization of orographic precipitation: an air-flow scheme and a cloud microphysical model. As is implied by an aggregation approach, the model does not carry any information on the geographical locations of the surface elevation classes within a grid cell. An air-flow model that merely determines the degree of uplifting of an air parcel as it passes over a mountain barrier would be consistent with the simplicity of this subgrid surface topographical representation. Such a model would not be able to capture the sequence and details of air-flow over a mountain, but would still provide useful information for stable orographic cloud where precipitation is mainly generated by the lifting and condensation of the moisture-rich air in the lower atmosphere (Cotton and Anthes, 1989). This approach would therefore deem to be most

useful for simulating winter-time precipitation along coastal mountain ranges.

Whether air flows over or around mountains depends on their height with respect to the grid-cell mean surface elevation, their horizontal dimension perpendicular and parallel to the upstream flow, the upstream wind speed, and the static stability. A fundamental parameter that controls upstream blocking is the Froude number, defined as

$$F_{\tau} = U/NH \tag{1}$$

where U is the upstream wind speed, N is the Brunt-Vaisala frequency and H is the relative height of the mountain. The square of the Froude number can be interpreted as the ratio of the kinetic energy of an air parcel to the potential energy required to lift the parcel from the surface to the mountain top. Analytic theory (Sheppard, 1956; Smith, 1980,1988,1989) and high-resolution numerical modeling studies (Pierrehumbert and Wyman, 1985; Smolarkiewicz and Rotunno, 1989, 1990) have shown that air generally flows over mountain when the Froude number is large, but around it when the opposite. We have adopted a method that determines the height rise of an air parcel by its energy balance. An air parcel will be forced to lift over the mountain until all its kinetic energy is converted to potential energy, after which it simply flows around the mountain until it descends. Therefore, the maximum height rise attainable by an air parcel is given by  $h_{max} = U/N$ . This is schematically illustrated in Figure 1. The actual height rise, h, would be limited by the relative height of the surface elevation where the air parcel originates to the elevation of the mountain it encounters. Hence,

$$h = min(z_s - \bar{z}_s, h_{max}) \tag{2}$$

where  $z_s$  is the height of the surface elevation class of which the air parcel is being considered, and  $\bar{z}_s$  is the height of the grid cell mean surface elevation.

Once the height rise or descent of an air parcel is determined, values of the cloud variables in each elevation class can be diagnosed from profiles of those variables in the grid cell mean. The thermodynamic and cloud variables  $\theta_c$  and  $r_w$  are used in this procedure because of their conservative properties during condensation as well as advection. They are defined as

$$\theta_c = \theta - (L/c_p)(r_c/E) \tag{3}$$

$$r_w = r_v + r_c \tag{4}$$

where  $\theta = T/E$  is the potential temperature,  $E = (p/p_0)^{\kappa}$  with  $\kappa = R/c_p$  is the Exner function, and  $r_c$  and  $r_v$  are the mixing ratios of cloud and water vapor respectively. Profiles of  $\theta_c$  and  $r_w$  are interpolated from the grid cell mean to each elevation class according to the height rise/descent of the air parcel determined by the air-flow scheme.

For cloud microphysical calculations, the temperature T, cloud water  $r_c$  and water vapor  $r_v$  will be diagnosed from  $\theta_c$ ,  $r_w$  and the pressure p by assuming  $r_v$  never exceeds the water vapor saturation mixing ratio  $r_s(T,p)$ . Here the pressure p for each elevation class is estimated from its surface pressure  $p_s$ , which can be inferred from the grid cell mean surface pressure  $\bar{p}_s$  using the linearized hydrostatic relation

$$p_s = \bar{p}_s e^{-(z_s - \bar{z}_s)/\bar{H}} \tag{5}$$

where  $\bar{H}$  is the scale height. Therefore, elevation classes with higher surface elevations have lower surface pressures, which from the definition of  $\theta_c$  yield colder temperatures and higher cloud water concentrations.

The above procedures can be implemented either diagnostically or prognostically to account for subgrid cloud processes due to variations in surface elevations. In the former approach, cloud variables for each surface elevation class are diagnosed from the grid cell mean values at the beginning of each time step and cloud microphysical processes are calculated for each class accordingly. Because some microphysical processes such as

precipitation operate on time scales much shorter than advection,  $\theta_c$  and  $r_w$  may not be conserved in these procedures. Indeed, a preliminary testing of this approach resulted in orographic signatures of precipitation that are far too strong, violating the conservation of energy and water budgets. An approach that carries  $\theta_c$  and  $r_w$  prognostically for each elevation class as well as the grid cell mean avoids this problem. To implement such an approach, tendencies in  $\theta_c$  and  $r_w$  due to air flow over or around mountain will be calculated for each elevation class. The calculation is based on the difference between the vertical profiles of those variables for the grid cell mean and those diagnosed for each surface elevation class from the air-flow scheme. The tendencies also depend on the time scale over which the lifting/descent completes. Physically this time scale,  $\tau$ , depends on the wind speed as well as the spatial distribution of the surface elevation classes within the domain grid cells. As a first test of the aggregation scheme, it is treated as an adjustable parameter in this study.

The parameterization described has been implemented into the PNL regional climate model. Advection and horizontal diffusion are calculated based on the grid-cell mean variables and applied to the prognostic equations of both the grid-cell means and the individual elevation classes. Physical processes such as radiation, planetary boundary layer and surface physics, cloud microphysics and cumulus convection are all performed for each elevation class. Tendencies from these processes are applied to prognostic equations for each class and then aggregated to the grid-cell mean variables.

Although the scheme described here offers some solutions to the problem of representing subgrid scale orographic effects on clouds, it does not solve all of the difficulties. Most notably the rainshadowing effect that results from dry-adiabatic descent of air on the lee side of mountains is not accounted for on the subgrid scale by this parameterization. The lee side of the mountains receive the same precipitation as the upwind side if they belong to elevation classes within the same grid cell. This is not a problem for narrow ridges with advective time scales shorter than the time scales of precipitation processes, but is potentially a serious limitation for broader orographic features not explicitly resolved by the regional model. In short, the grid resolution of the regional model should be chosen to be fine enough that the advective time scale is shorter than that of the formation of

precipitation.

### 3. RESULTS

We have implemented the subgrid parameterization of orographic precipitation into the PNL regional climate model. The coarse and fine mesh used in this study are shown in Figure 2. The horizontal resolution of the coarse and the fine domains is 90 km and 30 km, respectively. The model has 23 vertical layers. A one-year simulation has been completed in the nested configuration without any aggregation for evaluating the general performance of the model. We will identify the model results for the coarse and fine domains in this simulation by CN and FN, respectively. For testing of the aggregation scheme, a onemonth simulation has been performed over the same coarse domain shown in Figure 2. The aggregation of surface elevation classes are carried out over an area slightly larger than the nested domain indicated in the same figure. This simulation will be identified by CAGG. All simulations are performed with the same physical parameterizations and lateral boundary conditions from ECMWF analysis. Model results will be compared with observations made at more than 500 weather stations in the Pacific Northwest (Figure 3). Evaluation of the models will center on fields measured by these stations: daily maximum and minimum surface temperatures, and precipitation. Snotel stations that record snow cover over the same region will also be used for comparison.

### (a) Nested Simulation Without Aggregation

To evaluate the performance of the regional climate model, a one-year simulation (October 1987 - September 1988) has been completed with the nested configuration described above. Only model results from the nested domain (FN) are used here. Comparison of model and observations are made by interpolating model simulated values to the exact locations of weather stations shown in Figure 3 from the closest four grid points surrounding them.

Figure 4 shows the observed and model simulated monthly averaged surface temperatures and precipitation averaged over all the weather station locations. The model is capable of simulating the seasonal cycle in the surface temperature with a bias of about 2° C. Maxima in the precipitation during winter and early spring are also simulated well by the model.

To evaluate the model performance beyond regional average, Figure 5 shows scatter plots of model versus observed temperatures and precipitation for all stations during January and July of 1988. During winter time, little bias is found in either the surface temperatures or the precipitation. The model explains between 50-75% of the spatial variance in the observations made over a wide variety of atmospheric conditions and surface boundaries. During summer time, precipitation is generated more randomly at different locations by convective instability. Comparison of modeled and observed precipitation on a point-by-point basis indicates very little skill, consistent with the physical processes that are at play. With BATS implemented in the model, snow cover is also simulated and saved daily. A comparison of the simulated and observed snow cover (in inches of water equivalence) is shown in Figure 6 as scatter plot for December 1987. Not only is there little correlation between the observed and model simulated snow cover, the bias in the mean values is also significant. It is clear that the simulation of snow cover has to be improved for credible modeling of surface hydrological processes.

### (b) Testing of Aggregation Scheme

Short simulations of 5 days each were performed to test the sensitivity of the aggregation scheme to the parameter,  $\tau$ , which controls the time scale for the air-flow over mountains. We tested a range of values for  $\tau$  between 2 hours to 6 hours. Figure 7 shows a eastwest cross section of three grid cells in western Washington State, covering the Olympic Mountain, the Puget Sound and the Cascade mountain range. Surface elevation varies from sea level to above 2000 m in the mountains. The model simulates precipitation for each elevation class within a grid cell. The precipitation is then distributed back to the geographical locations according to the 1.5 km high resolution surface elevation data from which information of the aggregation scheme was derived. Interpolation has been performed for the simulated precipitation between elevation classes on adjacent grid cells. This ensures more continuous spatial distribution of precipitation in transition from one grid cell to another. Consistent with the physical interpretation of the parameter, the figure shows stronger orographic signatures for smaller values of  $\tau$ .

The one-month simulation with the aggregation scheme (CAGG) is based on  $\tau$  equals

6 hours. Figure 8 shows the same cross section as in Figure 7 over the Puget Sound area, for model simulated rainfall, snowfall and snow cover. Corresponding values for the CN simulation are shown in the same for comparisons. The orographic signatures in the CAGG simulation are very similar to what are usually observed in mountainous areas, with increases in precipitation on the windward side and the rainshadowing effect on the lee side. Also snow cover are now being simulated with reasonable magnitude. Figure 9 shows the spatial distribution of precipitation simulated with the aggregation scheme. Much more spatial detail is now captured by the model than would have been by the 90-km grid without aggregation. In this particular simulation, effects of surface topography on precipitation are strongest on the western Cascades.

Figure 10 shows scatter plots similar to Figure 5 for model simulations with the aggregation scheme (CAGG) and those of the coarse (CN) and fine domain (FN) without the aggregation scheme. With the aggregation scheme, the model is capable of simulating the stronger precipitation events that occur mostly on higher elevations. The correlation coefficients, r, are calculated for each scatter plot. More skill is demonstrated with the use of the aggregation scheme than even the 30 km nested simulation. This represents a significant improvement in representing subgrid orographic precipitation, not only in terms of improved skill, but also computational efficiency. A one-day simulation for the model with aggregation takes 2.5 CPU hours on an IBM RS/6000-560 in contrast to the 8.5 CPU hours for the nested configuration. Finally, the simulated snow cover for cases CAGG is shown in Figure 11. Although there is still a lot of scatter, the performance of the model with aggregation clearly surpasses that of the fine domain simulation (FN) shown in Figure 6.

### 4. DISCUSSION

An aggregation scheme has been developed for climate models to represent subgrid effects of topography on precipitation and snow cover. With a simple air-flow scheme and a detailed mixed-phase cloud microphysics scheme, cloud and surface processes are calculated for all subgrid elevation classes. Results indicate that such an approach is capable of capturing the enhancement of precipitation due to uplifting of air parcels by underlying

mountain barriers. The simulated spatial distribution of precipitation and snow cover shows realistic climatological features typical of mountainous area. Rainshadow effects are resolved only on the scales of the model grid size, but not for mountain ranges within a grid cell. This, however, does not seem to have an adverse effect in this simulation where most precipitation falls on mountain ranges along the coast. These mountains tend to be narrow enough that the time scale for advection is much shorter than that of the precipitation processes. More testing is needed to determine an optimal horizontal resolution for resolving rainshadow effects on broader mountain ranges such as in the Rockies.

Despite the preliminary success demonstrated in this study, the aggregation scheme can now at best simulate the most general climatological features of orographic precipitation. There are inherent limitations in the aggregation approach because no information of the geographical orientation of the surface elevations is carried by the model. Physical processes related to the more detailed air circulation such as lee waves and local thermally driven circulations cannot be represented by such a method. Nevertheless, several aspects of the model can be further improved within the present framework for more realistic representations of the air circulation. These include a more detailed method for determining the height rise of air parcels over mountain barriers, the use of a more physically based time scale parameter, and possibly, the utilization of more information related to the aggregation of surface elevation. This study represents an important step toward the development of subgrid parameterizations that are essential even for regional climate models or global climate models of the future. The enhanced information produced from these parameterizations is valuable as climate inputs to models of surface hydrological processes.

Acknowlegements. This work is supported by Laboratory Directed Research and Development funding from the Pacific Northwest Laboratory. Pacific Northwest Laboratory is operated for the U.S. Department of Energy by Battelle Memorial Institute under Contract DE-AC06-76RLO 1830.

### REFERENCES

Anthes, R.A., E.Y. Hsie, and Y.H. Kuo. 1987. Description of the Penn State/NCAR Mesoscale Model Version 4 (MM4). NCAR Technical Note, NCAR/TN-282+STR.

Barros, A.P. and D.P. Lettenmaier. 1993. Dynamic Modeling of Orographically-Induced Precipitation. Rev. Geophys. In Press.

Bergeron, T. 1960. Problems and Methods of Rainfall Investigation. <u>Geophysical Monographs</u>. <u>5</u>:5-30.

Browning, K.A. 1980. Structure, Mechanism and Prediction of Orographically-Enhanced Rain in Britain. Orographic Effects in Planetary Flows. <u>GARP Publications Series</u>. 23:88-108.

—, C.W. Pardoe, and F.F. Hill. 1975. The Nature of Orographic Rain at Wintertime Cold Fronts. Quart. J. Roy. Meteor. Soc. 101:333-352.

Choularton, T.W. and S.J. Perry. 1986. A Model of the Orographic Enhancement of Snowfall by the Seeder-Feeder Mechanism. Quart. J. Roy. Meteor. Soc. 112:335-345.

Cotton, W.R. and R.A. Anthes. 1989. Storm and Cloud Dynamics. Academic Press.

—, G.J. Tripoli, R.M. Rauber, and E.A. Mulvihill. 1986. Numerical Simulation of the Effects of Varying Ice Crystal Nucleation Rates and Aggregation Processes on Orographic Snowfall. <u>J. Climate Appl. Meteor.</u> 25:1658-1680

Dickinson, R.E., R.M. Errico, F. Giorgi, and G.T. Bates. 1989. A Regional Climate Model for the Western U.S. Clim. Change. 15:383-422.

—, A. Henderson-Sellers, P.J. Kennedy, and M.F. Wilson. 1986. Biosphere-Atmosphere Transfer Scheme (BATS) for the NCAR Community Climate Model. <u>NCAR Technical Note</u>, <u>NCAR/TN-275+STR</u>.

Fraser, A.B., R.C. Easter, and P.V. Hobbs. 1973. A Theoretical Study of the Flow of

Air and Fallout of Solid Precipitation Over Mountainous Terrain: Part I. Airflow Model. J. Atmos. Sci. 30:801-812.

Ghan, S.J., and R.C. Easter. 1992. Computationally Efficient Approximations to Stratiform Cloud Parameterization. <u>Mon. Wea. Rev.</u> 120:1572-1582.

Giorgi, F., G.T. Bates, and S.J. Nieman. 1993. The Multiyear Surface Climatology of a Regional Atmospheric Model over the Western United States. <u>J. Climate</u>. <u>6</u>:75-95.

—, —, and —. 1992. Simulation of the Arid Climate of the Southern Great Basin Using a Regional Climate Model. <u>Bull. Amer. Met. Soc.</u> 73:1807-1822.

—, and —. 1989. On the Climatological Skill of a Regional Model over Complex Terrain. Mon. Wea. Rev. 119:2870-2888.

Grell, G. 1993. Prognostic Evaluation of Assumptions Used by Cumulus Parameterizations. Mon. Wea. Rev. 121:764-787.

Grotch, S.L. and M.C. MacCracken. 1991. The use of General Circulation Models to Predict Regional Climatic Change. <u>J. Climate</u>. <u>4</u>:286-303.

Hobbs, P.V., R.C. Easter, and A.B. Fraser. 1973. A Theoretical Study of the Flow of Air and Fallout of Solid Precipitation Over Mountainous Terrain: Part II. Microphysics. J. Atmos. Sci. 30:813-823.

IPCC. 1991. Climate Change: The IPCC Scientific Assessment. Cambridge, UK.

Kiehl, J.T., R.J. Wolski, B.P. Briegleb, and V. Ramanathan. 1987. Documentation of Radiation and Cloud Routines in the NCAR Community Climate Model (CCM1). NCAR Technical Note, NCAR/TN-288+IA.

Madala, R.V. 1987. Efficient Time Integration Schemes for Atmosphere and Ocean Models. <u>Finite-Difference Techniques for Vectorized Fluid Dynamics Calculations.</u> D.L. Book, Ed. Springer-Verlag.

Pierrehumbert, R.T. and B. Wyman. 1985. Upstream Effects of Mesoscale Mountains. J. Atmos. Sci. 42:977-1003.

Sheppard, P.S. 1956. Airflow over Mountains. Quart. J. Roy. Meteor. Soc. 82:528-529.

Smith, R.B. 1989. Mountain Induced Stagnation Points in Hydrostatic Flows. <u>Tellus</u>. 41A:270-274.

- —. 1988. Linear Theory of Hydrostatic Flow Over An Isolated Mountain in Isoteric Coordinates. <u>J. Atmos. Sci. 45</u>:3889-3896.
- —. 1987. The Role of Moist Processes in Mountain Effects. Seminar/Workshop 1986 on Observation. Theory and Modelling of Orographic Effects. <u>European Center for Medium Range Weather Forecasts</u>. 1:77-111.
- —. 1980. Linear Theory of Stratified Hydrostatic Flow Past an Isolated Mountain. <u>Tellus</u>. 32:348-364.

Smolarkiewicz, P.K. and R. Rotunno. 1990. Low Froude Number Flow Past Three Dimensional Obstacles. Part II: Upwind Flow Reversal Zone. <u>J. Atmos. Sci.</u> 47:1498-1511.

— and —. 1989. Low Froude Number Flow Past Three Dimensional Obstacles. Part I: Baroclinically Generated Lee Vortices. <u>J. Atmos. Sci. 46</u>:1154-1164.

Storebo, P.B. 1975. Small Scale Topographical Influences on Precipitation. <u>Tellus</u>. <u>28</u>:45-59.

Sumner, G. 1988. Precipitation Process and Analysis. John Wiley & Sons.

Taylor, K.E. and S.J. Ghan. 1992. An Analysis of Cloud Liquid Water Feedback And Global Climate Sensitivity in a General Circulation Model. <u>J. Climate</u>. 5:907-919.

Tripoli, G.J. and W.R. Cotton. 1989. Numerical Study of an Observed Orogenic Convective System. Part I: Simulated Genesis and Comparison with Observations. Mon. Wea.

### Rev. 117:273-304.

— and —. 1986. An Intense, Quasi-Steady Thunderstorm Over Mountainous Terrain. Part IV: Three Dimensional Numerical Simulation. <u>J. Atmos. Sci.</u> 43:894-912.

Williamson, D.L., J.T. Kiehl, V. Ramanathan, R.E. Dickinson, and J.J. Hack. 1987. Description of NCAR Community Climate Model (CCM1). NCAR Technical Note, NCAR/TN-285 +STR.

Zhang, D.L. and R.A. Anthes. 1982. A High-Resolution Model of the Planetary Boundary Layer- Sensitivity Tests and Comparisons with SESAME-79 Data. <u>J. Appl. Meteor.</u> 21:1594-1609.

### FIGURE CAPTIONS

- Figure 1. A schematic illustration of air flow over mountain. The maximum height rise attainable by an air parcel is given by  $h_{max}$ . When lifting reaches the maximum, air flows around the mountain.
- Figure 2. Domains used in the regional climate simulations. The horizontal resolutions for the coarse and fine domains are 90 km and 30 km respectively.
- Figure 3. Locations of weather stations in the Pacific Northwest used in model evaluations.
- Figure 4. Simulated and observed monthly averaged daily maximum/minimum surface temperatures and precipitation averaged over all weather station locations. The simulation period is from October 1987 September 1988.
- Figure 5. Scatter plots of monthly averaged simulated versus observed daily maximum/minimum surface temperatures and precipitation for (a) January and (b) July of 1988.
- Figure 6. Scatter plot of monthly averaged simulated versus observed snow cover (December 1987) in inches of water equivalence. Observations are obtained from snotel stations across the Cascades and Northern Rockies in the Pacific Northwest.
- Figure 7. A east-west cross section of three model grid cells covering the Olympic Mountain, the Puget Sound and the Western Cascade Mountain. Solid represents the surface elevations defined by the elevation classes. The three dashlines represent precipitation simulated by the model using values of  $\tau$  ranging from 2 hours to 6 hours.
- Figure 8. The same east-west cross section as shown in Figure 7. The dashlines represent model simulated (a) rainfall, (b) snowfall, and (c) daily minimum surface temperature, and (d) snow cover. Simulated values shown are monthly averages of December 1987. The CN and CAGG simulations are represented by \*\* and \* respectively.
- Figure 9. Spatial distribution of the monthly-mean precipitation (mm/day) simulated by the model with aggregation. Each tic mark represents the 90 km horizontal resolution

used in the model.

Figure 10. Scatter plots of monthly averaged simulated versus observed precipitation in three simulations (a) 90-km grid with aggregation (CAGG), (b) 90-km grid withoug aggregation (CN), and (c) 30-km grid withoug aggregation (FN). Values for the correlation coefficient, r, are shown on the upper right corner of each scatter plot.

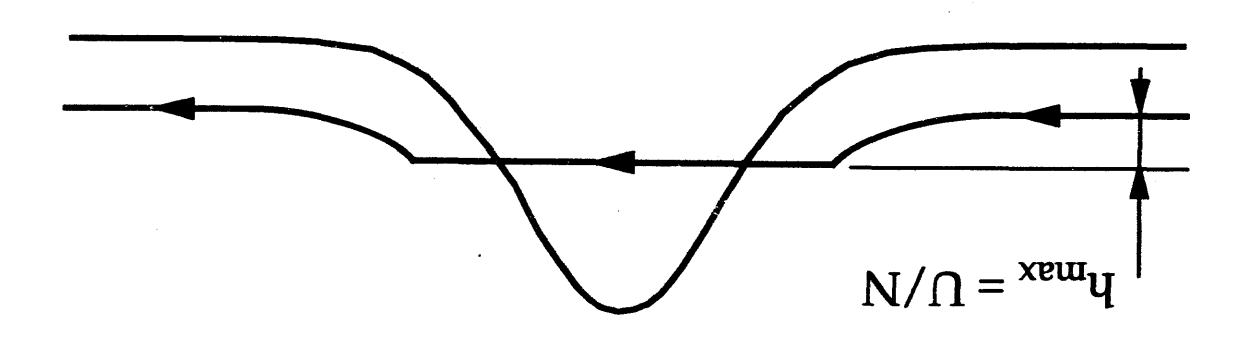
Figure 11. Scatter plot of monthly averaged simulated versus observed snow cover. Simulation is performed with the 90-km grid with aggregation. Thus is to be contrasted with Figure 6 for the 30-km grid simulation without aggregation.

## TIZT OF TABLES

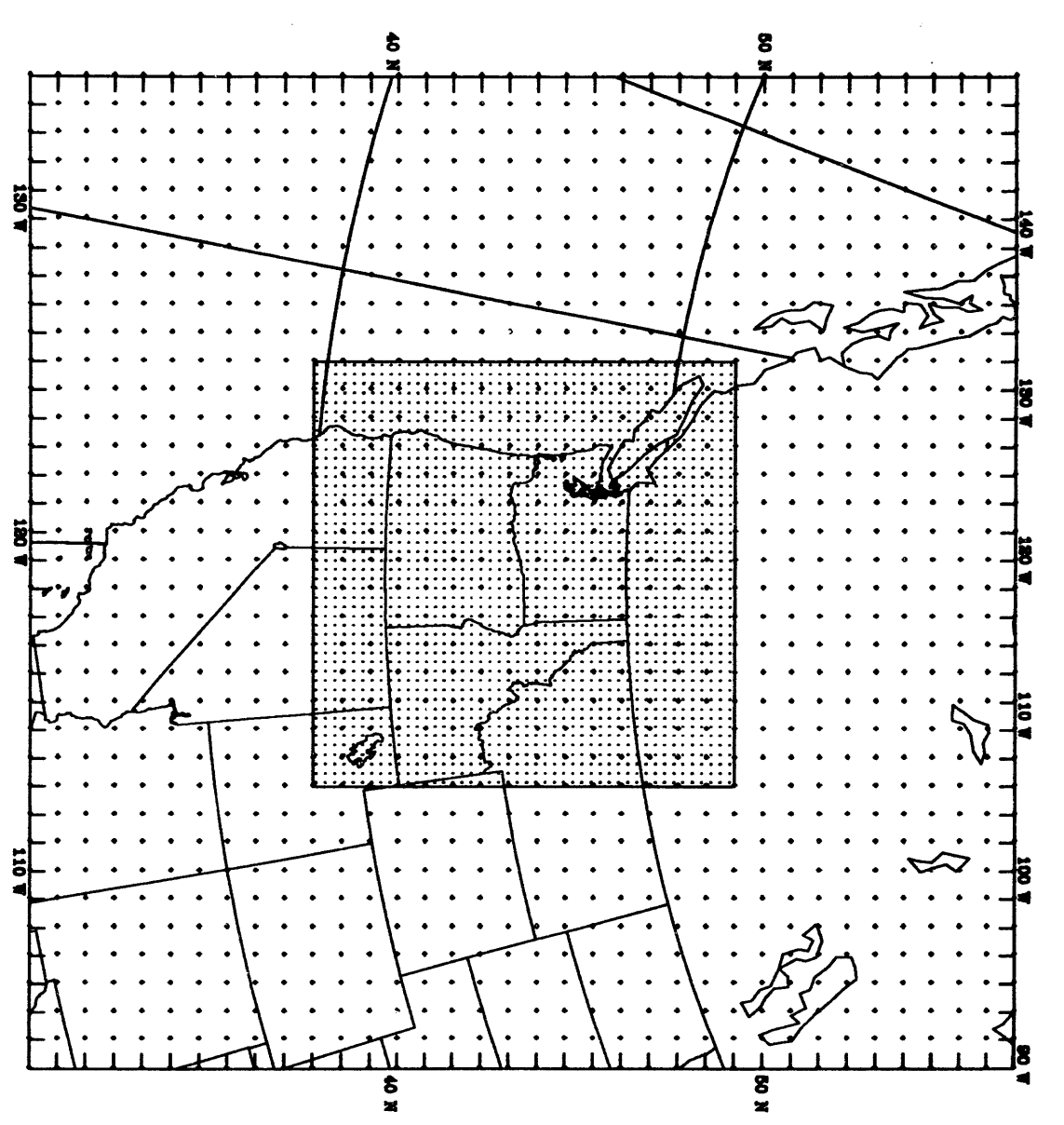
Table 1. The classification of surface elevations used in the subgrid parameterization.

Classification of Surface Elevations

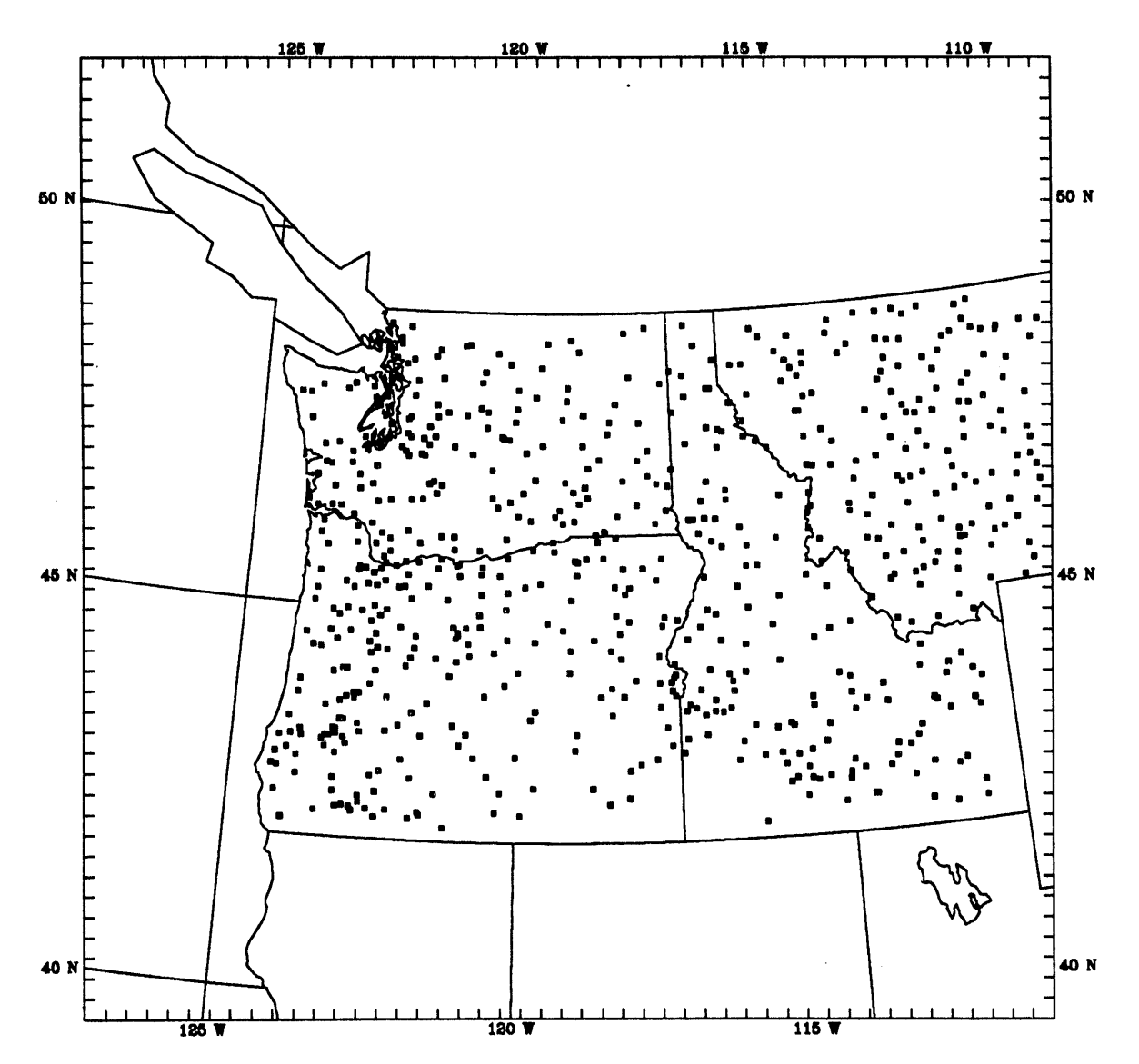
Class Number	Surface Elevation (m)
1	0-100
2	100-200
3	200-300
4	300-400
5	400-500
6	500-700
7	700-1000
8	1000-1500
9	1500-2000
10	2000-3000
11	3000-4000
12	4000-5000

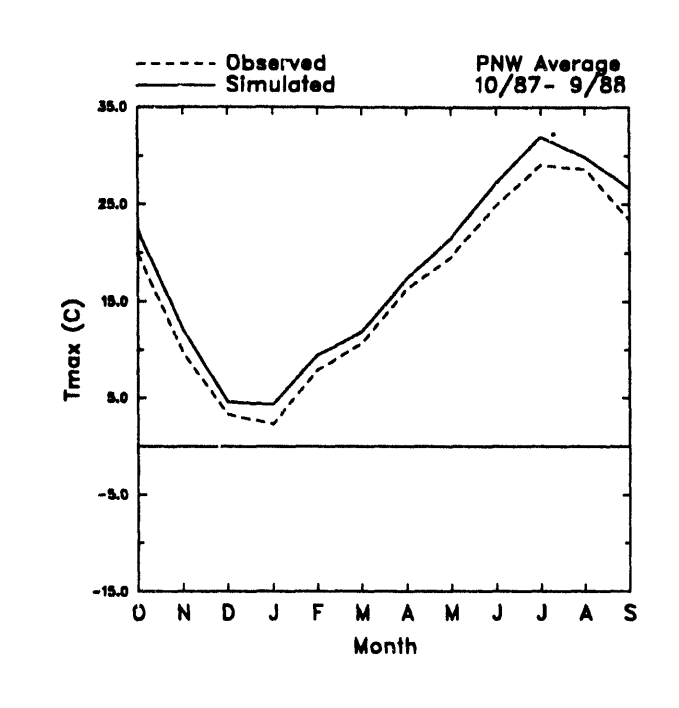


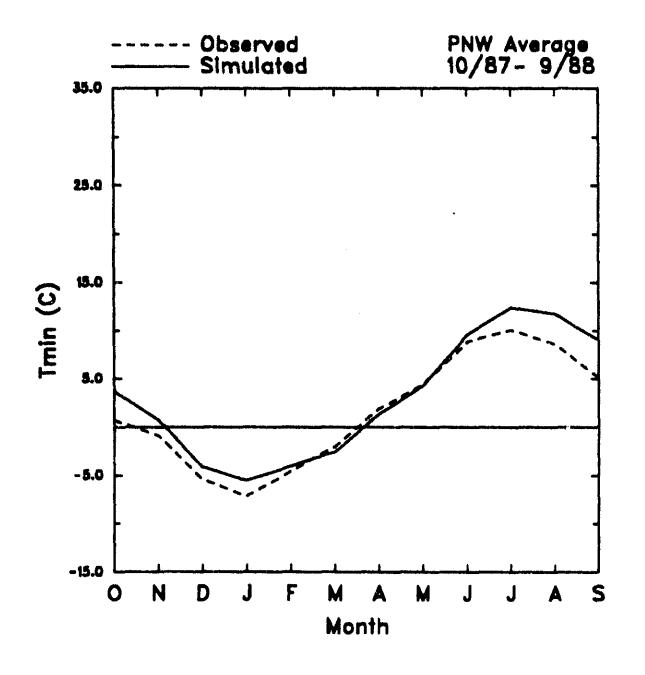
MM4 Model Domains

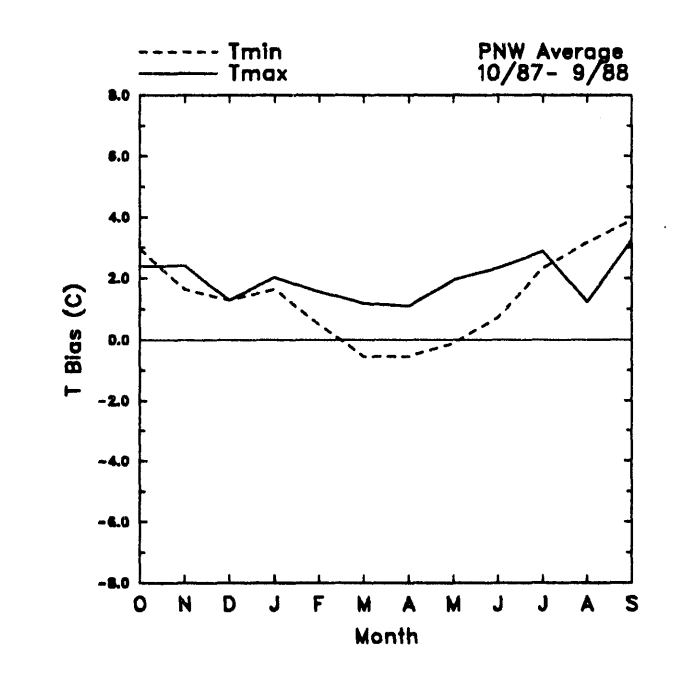


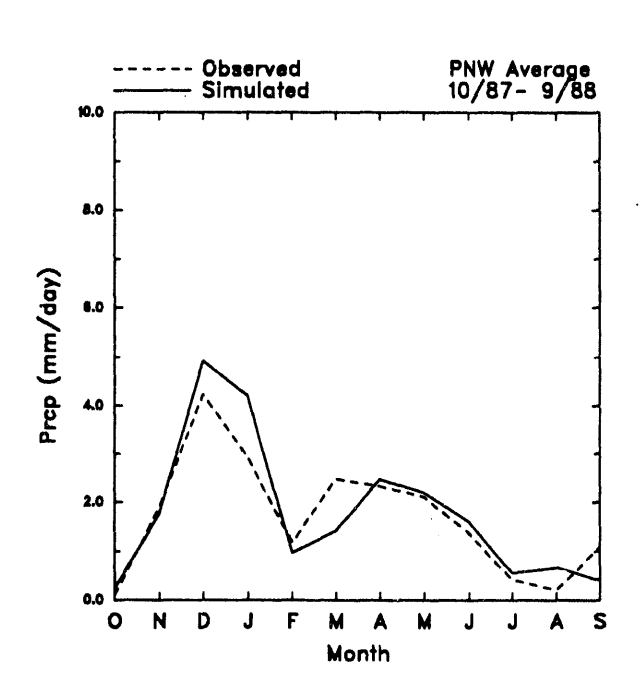
# Surface Station Locations

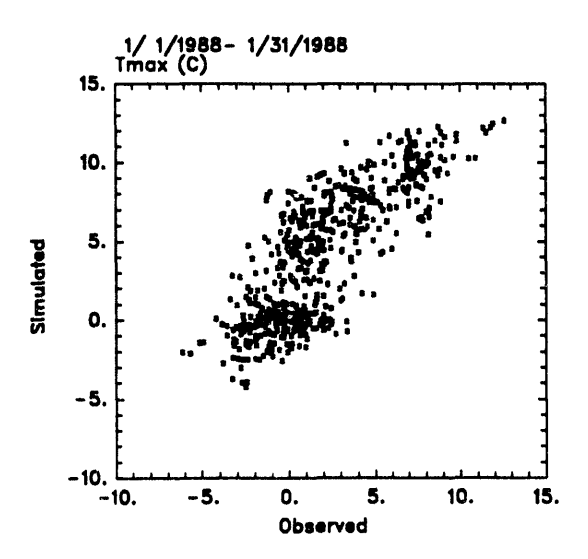


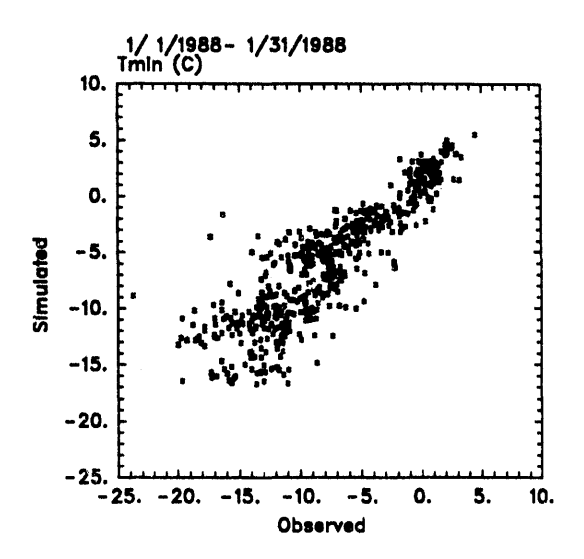


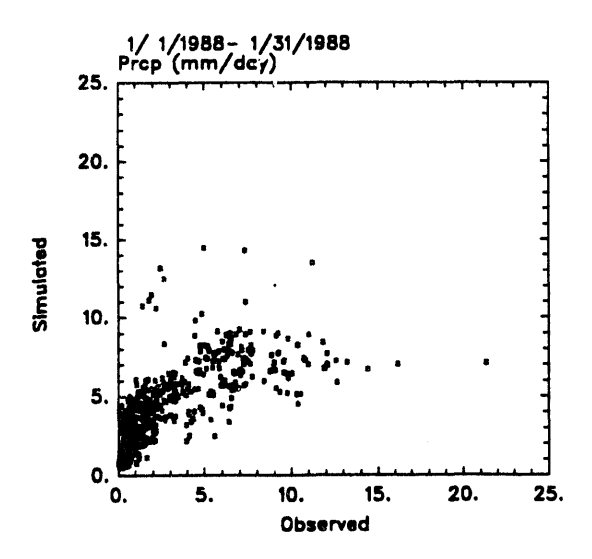


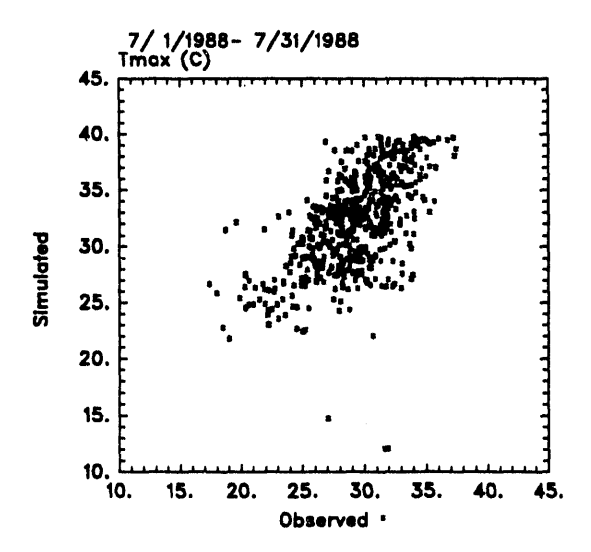


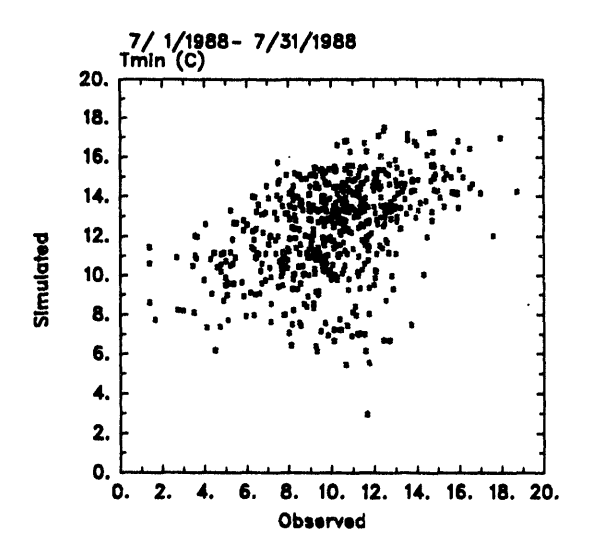


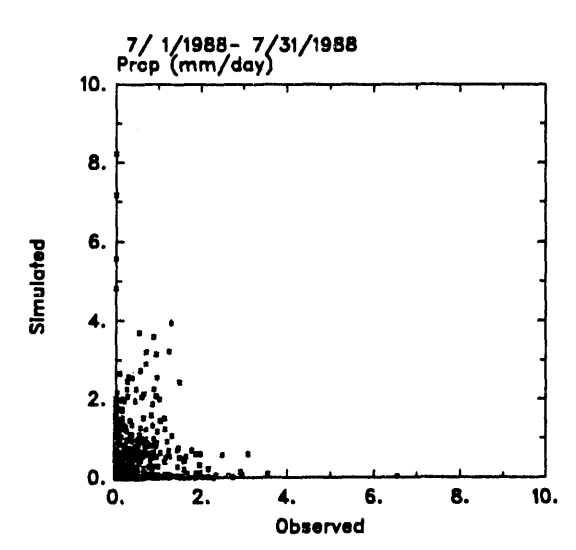


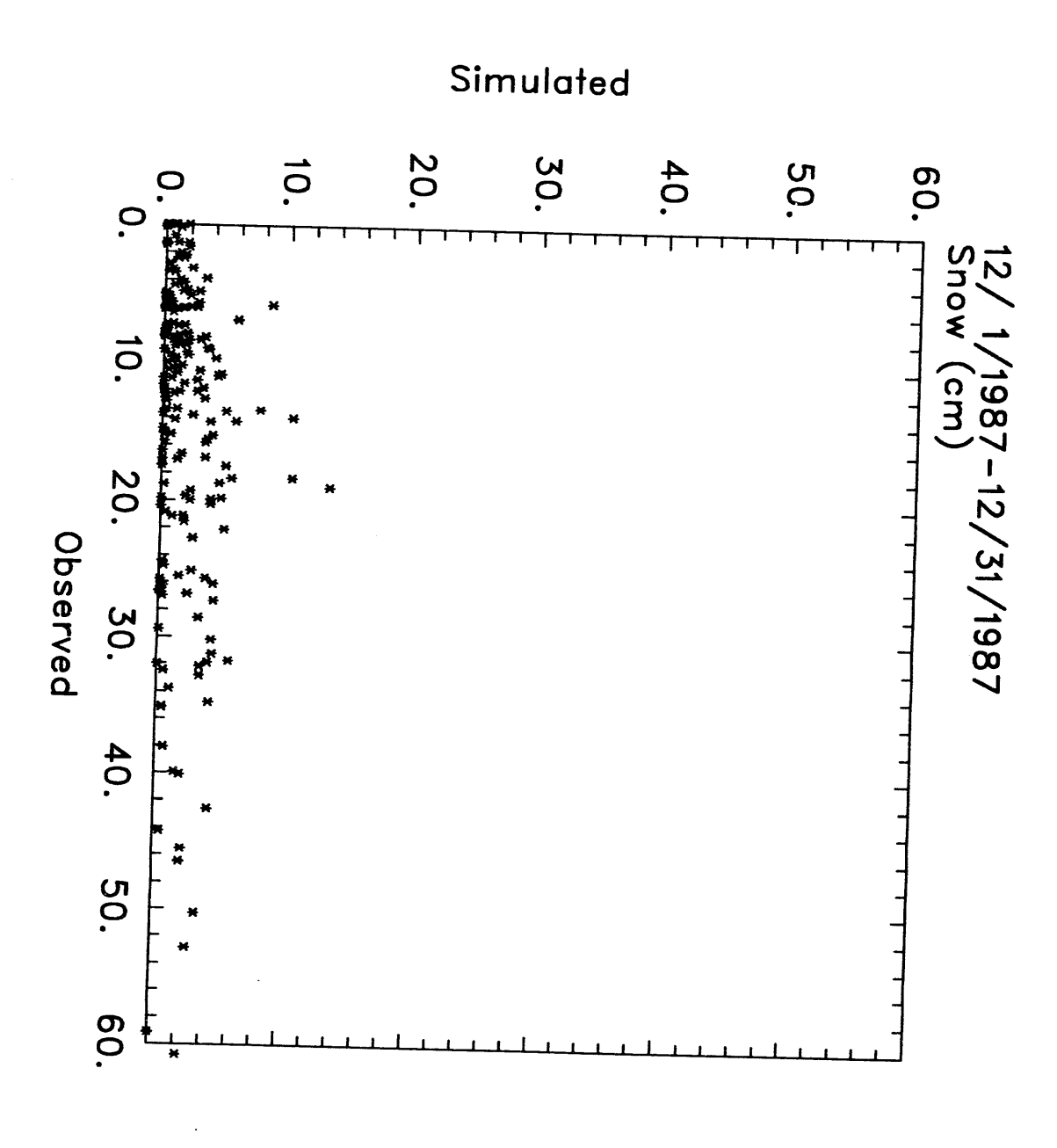


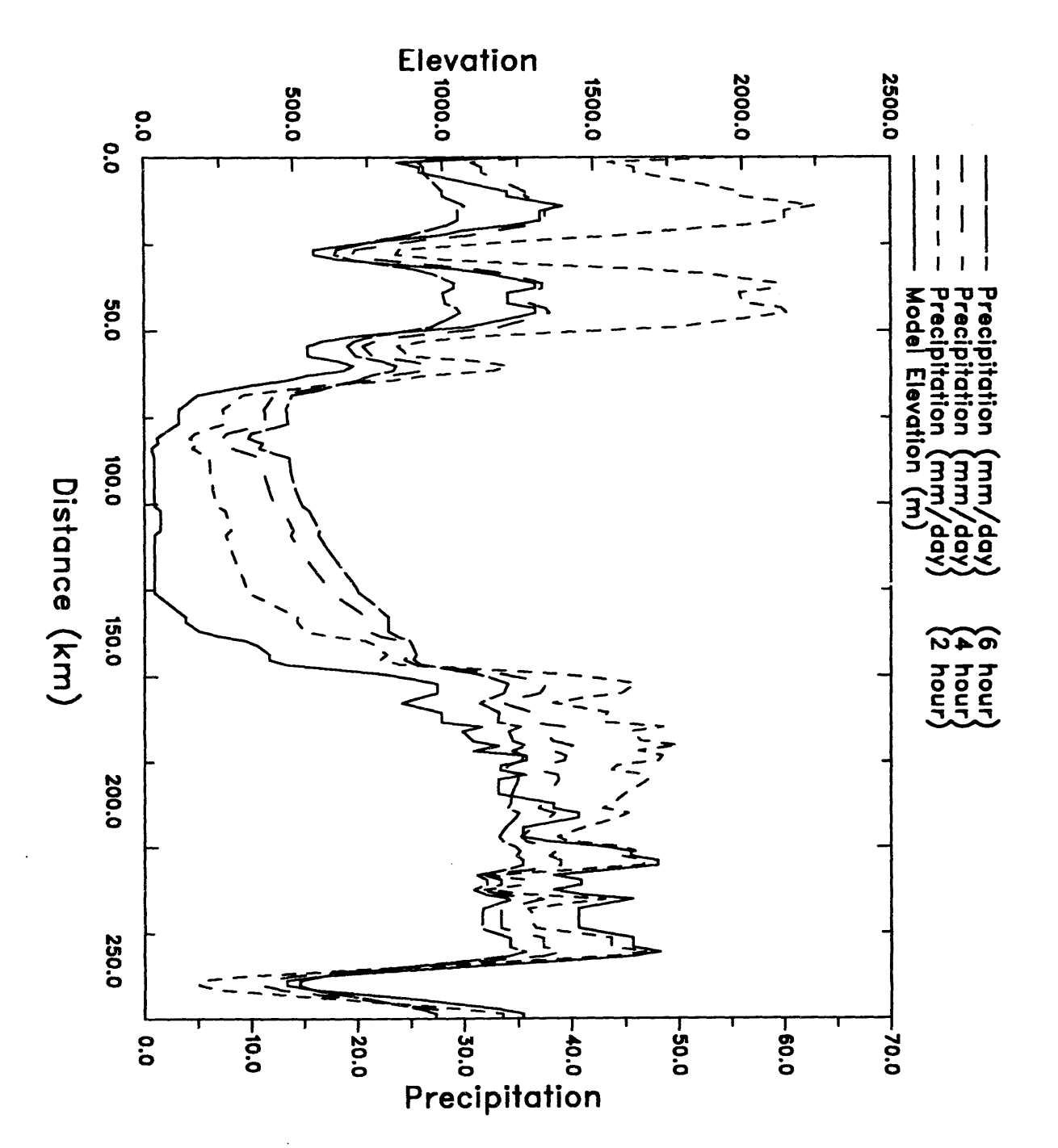


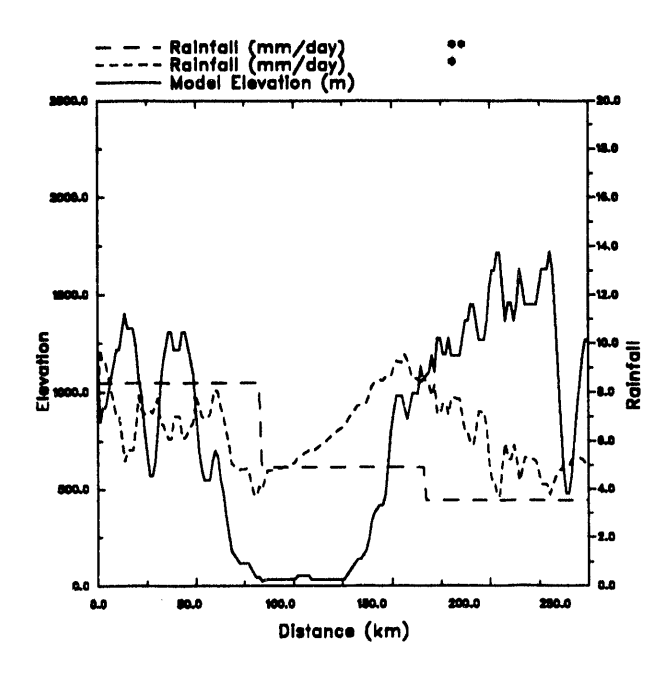


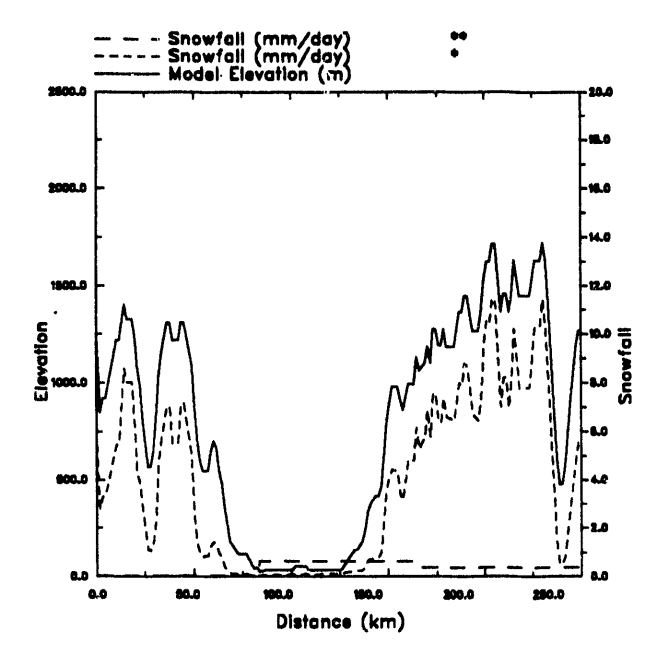


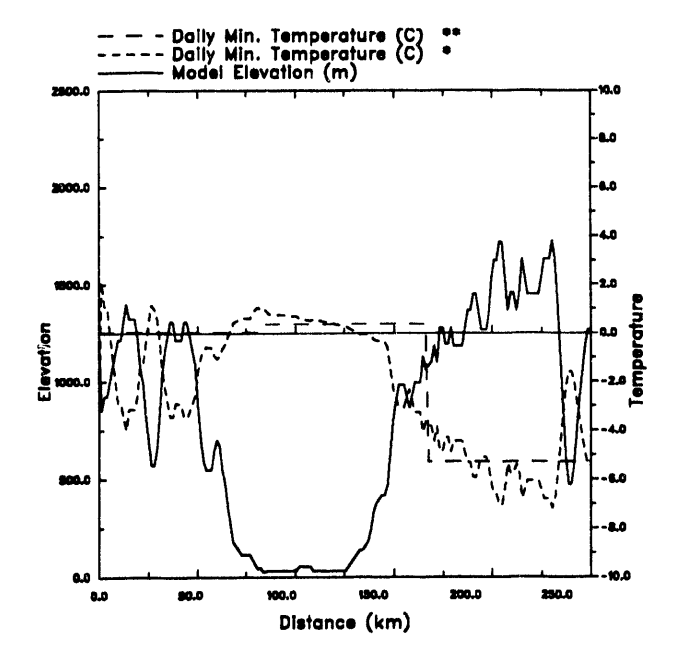


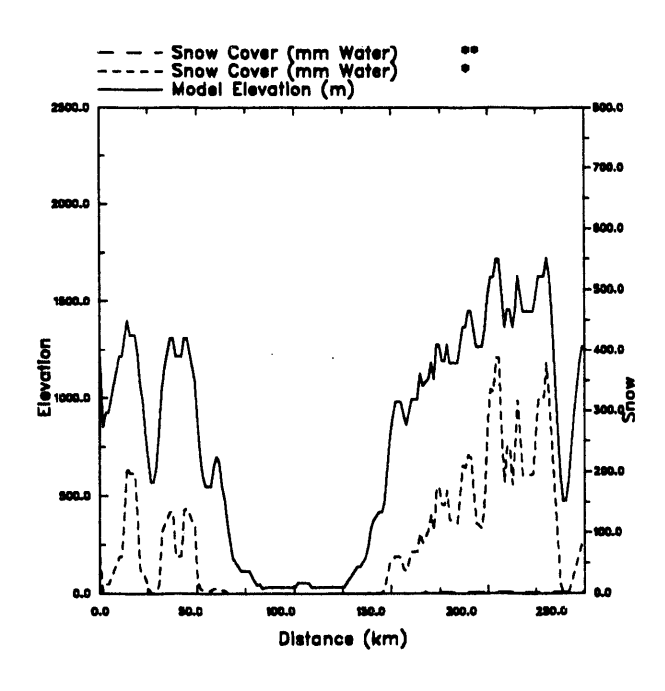


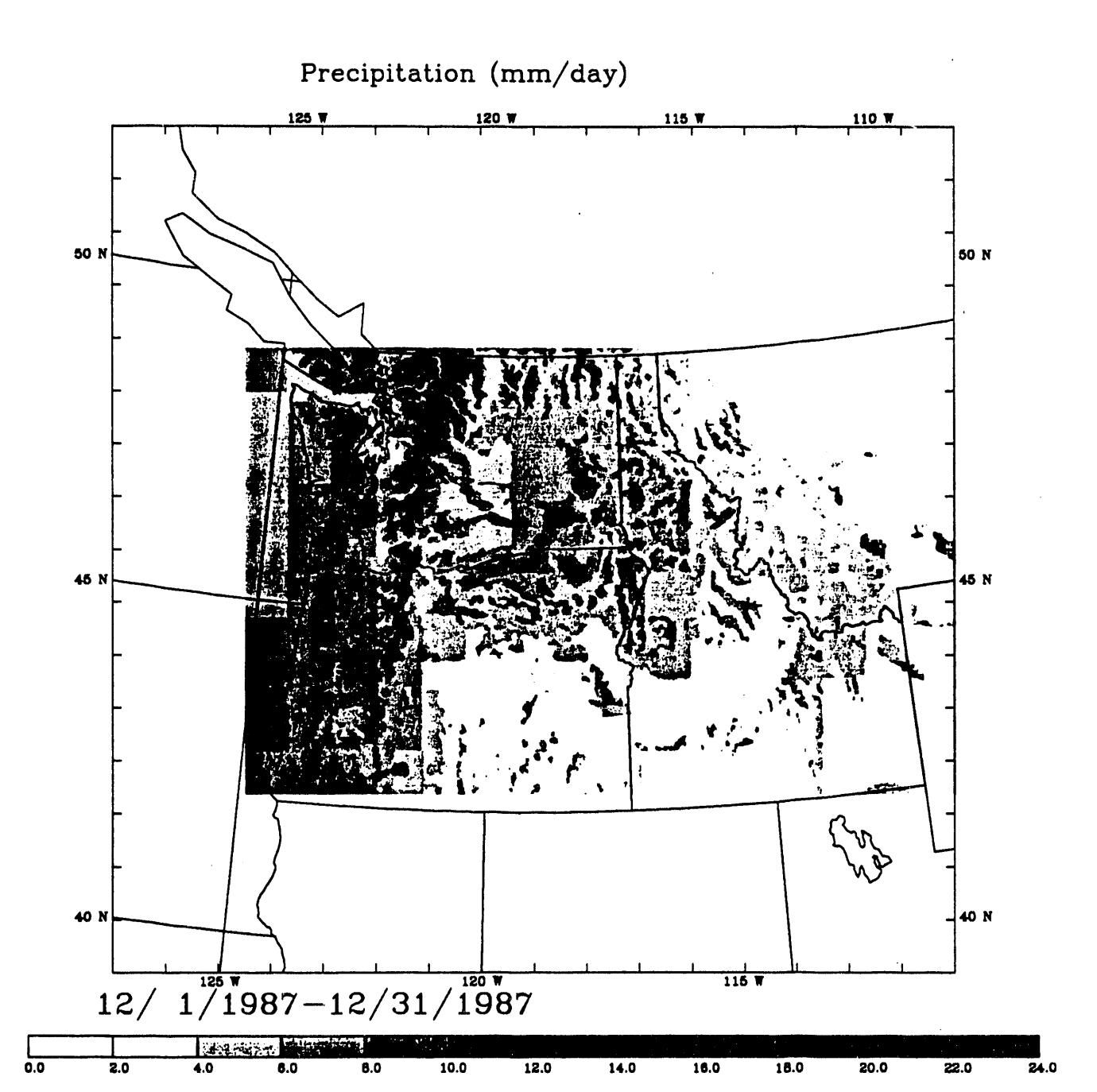


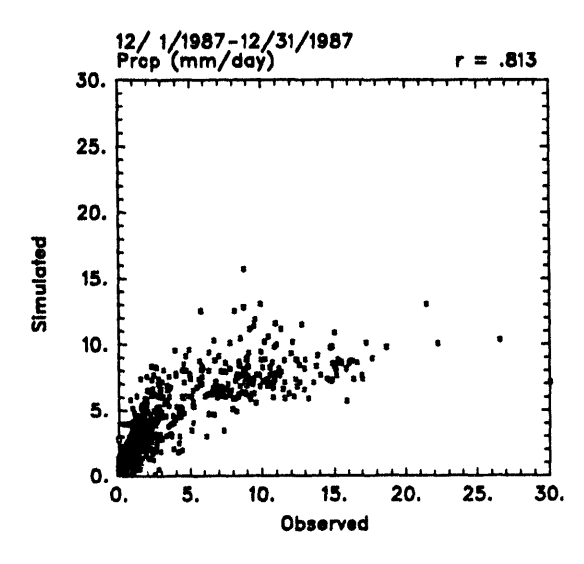


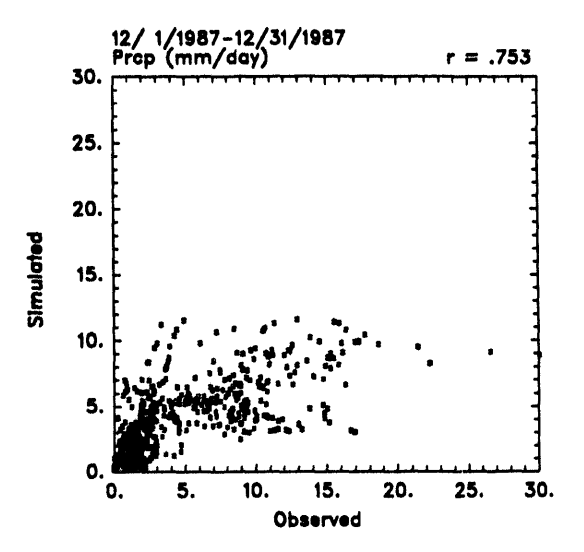


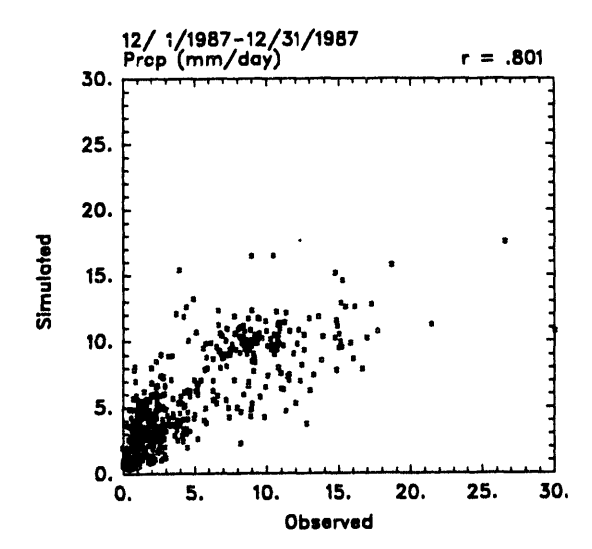


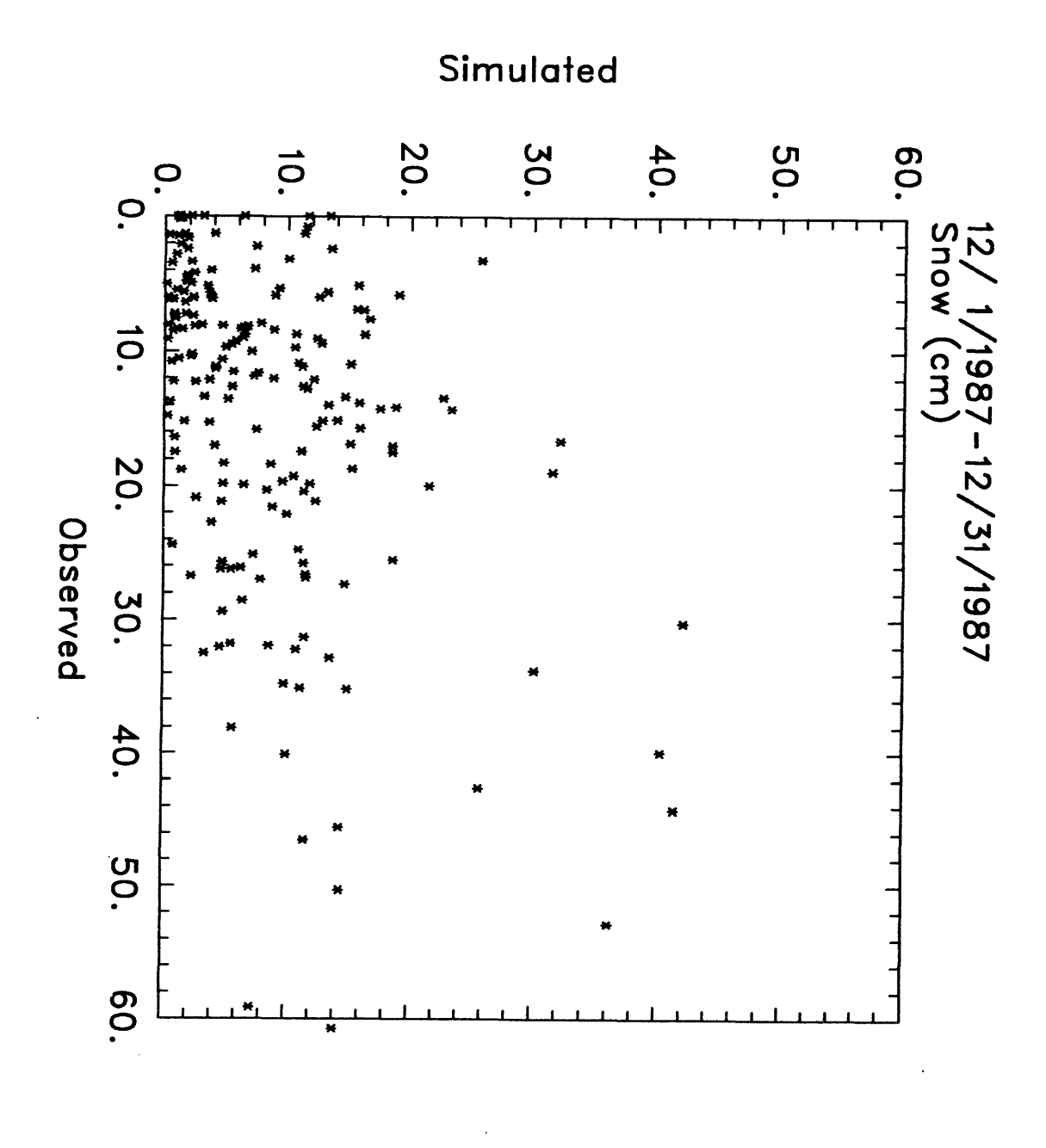












# DATE FILMED 6/22/94

